Analyzing and tailoring spectra of arbitrary microring resonator arrays based on six transfer cells and simulated annealing algorithm

Xiaobei Zhang (张小贝)*, Yunhong Ding (丁运鸿), Wei Hong (洪 伟), Xinliang Zhang (张新亮), and Dexiu Huang (黄德修)

Wuhan National Laboratory for Optoelectronics and School of Optoelectronics Science and Engineering, Huazhong University of Science and Technology, Wuhan 430074, China

**E-mail: hustzhang@gmail.com*

Received December 29, 2008

A simple approach based on six transfer cells and simulated annealing algorithm for analyzing and tailoring the spectra of arbitrary microring resonator arrays is presented. Coupling coefficients, ring sizes, and waveguide lengths of microring resonator arrays can be arbitrary in this approach. After developing this approach, several examples are demonstrated and optimized for various configurations of microring resonator arrays. Simulation results show that this approach is intuitive, efficient, and intelligent for applications based on microring resonator arrays.

OCIS codes: 230.4555, 230.5750, 230.3990.
doi: 10.3788/COL20090709.0841.

The single microring resonator has attracted lots of attentions on analysis, design, simulation, and fabrication, due to its unique merits such as high Q factor and free of facets for feedbacks[1−5]. Thus it is one of the most promising building blocks for future large-scale integrated optics. Various applications of the single microring resonator have been demonstrated in the fields such as optical filters, switches, modulators, sensors, and so on[6−9]. As the inherent limitation of the single microring resonator, the developing trend of this area is from a single microring resonator to multiple or array forms of microring resonators. There are already some demonstrations of series and parallel cascaded microring resonators[10,11]. Considerable attentions are paid to microring resonator arrays (MRAs) due to their improvements of spectra compared with a single microring resonator[12−14]. An analytical model for MRAs has been presented using Sylvester's theorem[12]. However, simplifying assumptions such as identical and lossless rings and identical coupling coefficients are adopted, which are not comprehensive for the analysis of practical MRAs. Furthermore, coupling coefficients are critical for spectral shapes. Generally, the coupling coefficients are not identical to tailor a specified spectrum. The simulated annealing algorithm[15] is a heuristic method that mathematically mirrors the cooling of a material to a state of minimum energy, which is suitable for optimization problems with multiple parameters. Previously it has been used for the optimization of pulse generations in MRAs[13], while the optimization of spectra has not been studied.

In this letter, we develop an approach based on six transfer cells and simulated annealing algorithm for analyzing and tailoring the spectra of MRAs. Six transfer cells are similar to our previous work[14]. However, the lengths of upper and lower waveguides here are modified to be different, which is the most general model for MRAs so far. The proposed approach is suitable for MRAs with arbitrary coupling coefficients, ring sizes, and waveguide lengths. Combined with the simulated annealing algorithm, a specified spectrum can be tailored with the maximal similarity by optimizing the coupling coefficients. After introducing the model and flow chart, we carry out some simulations as examples with various configurations of MRAs.

Figure 1(a) shows an $M \times N$ MRA with M rows and N columns, which is formed by N times parallel connections of M-series coupled microring resonators through lower and upper waveguides. The drop of the MRA appears at different sides depending on the parity of M, as shown in Fig. 1(a). Using a natural number coordinate system $n - m$, the microring resonator located at the mth row and the nth column can be denoted as MR(n, m). When the input is fixed at the left side of MR(N, 1), the elements of the MRA can be generally grouped into six classes, corresponding to couplers, ring resonators, and waveguides with two types due to different optical

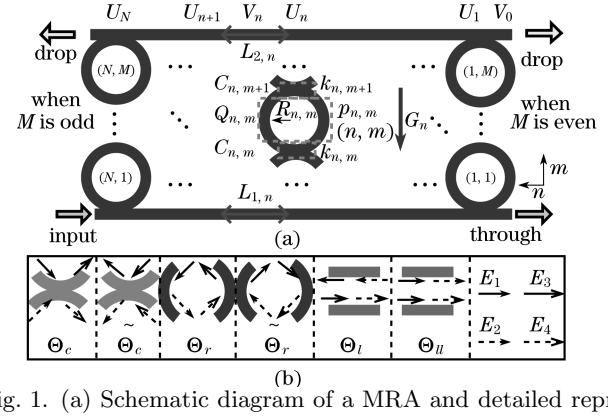

Fig. 1. (a) Schematic diagram of a MRA and detailed representation of the microring resonator at the mth row and the nth column. (b) Six transfer cells for the MRA and corresponding complex optical fields.

cycling directions, respectively, as shown in Fig. 1(b).

Following the transfer matrix formalisms, we adopt the six transfer cells to analyze MRAs. Complex optical fields in these six cells are denoted as E_1, E_2, E_3, and E_4. Then the transfer matrix can be represented as $(E_2; E_4) = \Theta(E_1; E_3)$. The corresponding set can be denoted as $\mathbf{\Theta} = \left\{ \Theta | \, \Theta \in \{\Theta_{\rm c}, \tilde{\Theta}_{\rm c}, \Theta_{\rm r}, \tilde{\Theta}_{\rm r}, \Theta_{\rm l}, \Theta_{\rm ll}\} \right\}$, while these six cells can be expressed as $\Theta_{\rm c}(k) = (i/k)\,(t, -1; 1, -t)$,$\tilde{\Theta}_{\rm c}(k) = (-i/k)\,(t, -1; 1, -t)$,$\Theta_{\rm r}(p) = \left(p, 0; 0, p^{-1}\right)$, $\tilde{\Theta}_{\rm r}(p) = \left(p^{-1}, 0; 0, p\right)$,$\Theta_{\rm l}(l_1, l_2) = \left(l_2^{-1}, 0; 0, l_1\right)$, and $\Theta_{\rm ll}(l_1, l_2) = (l_2, 0; 0, l_1)$. Here, $\Theta_{\rm c}$ and $\tilde{\Theta}_{\rm c}$ are wavelength independent, while the other four cells are wavelength dependent. t and k are the transmission and coupling coefficients, respectively, and $k^2 + t^2 = 1$ when the coupling process is lossless. The distances between lower and upper adjacent columns are L_1 and L_2, respectively, and the radius of resonator is R. The complex optical field change coefficients of the half round-trip resonator, the lower and upper waveguides are given by $p = \exp(\mathrm{i}\gamma_{\rm r}\pi R)$, $l_1 = \exp(\mathrm{i}\gamma_{\rm l} L_1)$, and $l_2 = \exp(i\gamma_{\rm l} L_2)$, respectively, where $\gamma_{\rm r} = \beta + \mathrm{i}\alpha_{\rm r}$ and $\gamma_{\rm l} = \beta + \mathrm{i}\alpha_{\rm l}$ are the complex propagation constants of ring resonators and straight waveguides, respectively; $\beta = 2\pi n_{\rm eff}/\lambda$ is the real part of complex propagation constants for both ring resonators and straight waveguides, $n_{\rm eff}$ is the effective index, and λ is the wavelength; $\alpha_{\rm r}$ and $\alpha_{\rm l}$ are amplitude attenuation coefficients for ring resonators and waveguides, respectively.

Figure 1(a) also shows the details of MR(n, m) , which can be generally decomposed into three subsections of two couplers and a ring resonator with transfer matrices $C_{n,m}$, $C_{n,m+1}$, and $Q_{n,m}$, respectively. The transmission coefficient $t_{n,m}$, the coupling coefficient $k_{n,m}$, and the resonator radius $R_{n,m}$ are not required to be identical for each resonator in our proposed approach. The complex optical field change coefficient of the half round-trip resonator is given by $p_{n,m} = \exp(\mathrm{i}\gamma_{\rm r}\pi R_{n,m})$. The transfer matrices of the components of MR(n, m) are given by

$$C_{n,m} = \begin{cases} \Theta_{\rm c}(k_{n,m}) & \text{for} \quad m = \text{odd} \\ \tilde{\Theta}_{\rm c}(k_{n,m}) & \text{for} \quad m = \text{even} \end{cases}, \tag{1a}$$

$$Q_{n,m} = \begin{cases} \Theta_{\rm r}(p_{n,m}) & \text{for} \quad m = \text{odd} \\ \tilde{\Theta}_{\rm r}(p_{n,m}) & \text{for} \quad m = \text{even} \end{cases}. \tag{1b}$$

After the processes of decompositions and syntheses, the longitudinal transfer matrix of the nth column is written as $G_n = \left(\prod_{m=1}^{M} C_{n,m} Q_{n,m} \right) C_{n,M+1}$. Then we can obtain the transverse transfer matrix of the nth column as

$$U_n = \left(-G_{n,11}, 1; (-1)^M, G_{n,22}\right)/G_{n,12}. \tag{2}$$

The transfer matrices of waveguides between the nth and $(n-1)$th columns with the lower and upper lengths $L_{1,n-1}$ and $L_{2,n-1}$ are expressed as

$$V_{n-1} = \begin{cases} \Theta_l(l_{1,n-1}, l_{2,n-1}) & \text{for} \quad M = \text{odd} \\ \Theta_{ll}(l_{1,n-1}, l_{2,n-1}) & \text{for} \quad M = \text{even} \end{cases}, \tag{3}$$

where $l_{1,n-1} = \exp(\mathrm{i}\gamma_{\rm l} L_{1,n-1})$ and $l_{2,n-1} = \exp(\mathrm{i}\gamma_{\rm l} L_{2,n-1})$ denote the complex optical field change coefficients of the lower and upper waveguides, respectively. If n=1, we adopt $L_{1,0} = L_{2,0} = 0$, and hence $l_{1,0} = l_{2,0} = 1$ and $V_0 = (1, 0; 0, 1)$ for convenience.

Finally, the total transfer matrix of the MRA can be obtained as $P = \prod_{n=1}^{N} V_{n-1} U_n$. Normalized complex transfer functions at the through port ζ_T and at the drop port $\zeta_{\rm D}$ can be expressed as

$$(\zeta_{\rm T}; \zeta_{\rm D}) = \begin{cases} \left(|P|; -P_{12}\right)/P_{11} & \text{for} \quad M = \text{odd} \\ (P_{22}; P_{12}) & \text{for} \quad M = \text{even} \end{cases}. \tag{4}$$

Corresponding transmission spectra are given as $T = |\zeta_{\rm T}|^2$ and $D = |\zeta_{\rm D}|^2$. When there is no loss, the sum of T and D equals unit due to the energy conservation, meaning that their spectra are complementary. In the following, only the spectra at the drop port are chosen to be studied for simplicity.

The above model can be used for analyzing an arbitrary MRA under given coupling coefficients, ring sizes, and waveguide lengths. For further tailoring the spectra, the coupling coefficients are required to be optimized for a given configuration. We denote the coupling coefficient matrix as

$$K = \begin{bmatrix} k_{1,1} & \cdots & k_{1,M+1} \\ \vdots & \ddots & \vdots \\ k_{N,1} & \cdots & k_{N,M+1} \end{bmatrix}. \tag{5}$$

In the simulation, the spectrum is discrete and W is the sampling number for a specified wavelength range. The target spectrum is denoted as $D^{\rm target}$, and then the cost function E of the spectrum D is defined as

$$E = \sum_{j=1}^{W} \left| D_j - D_j^{\rm target} \right|. \tag{6}$$

The temperature of the cooling process is denoted as $T_{\rm p}$. Figure 2 presents the flow chart of the simulated annealing algorithm for optimizing the coupling coefficients. At the beginning, a guess of K is given. Then a disturbed matrix K' is sent to calculate the change of the cost function $\delta E = E(K') - E(K)$. Using the classical simulated annealing algorithm[15], the temperature decreases after some iterative times at each temperature. The simulated annealing process is finished when the temperature decreases to the final temperature. During the process of cooling, we label three states 1, 0, and -1 to monitor the acceptance and rejection states, as shown in Fig. 2. They represent that the new value K' is accepted with a smaller cost function, rejected and accepted by a probability $\exp(-\delta E/T_{\rm p})$, respectively. Finally, the optimized coupling coefficient matrix is obtained. The optimization results may be multiple solutions due to the inherent principle of this algorithm.

Using the proposed approach, we calculate the transmission spectra of five configurations with different M and N, as shown in Fig. 3(a). Parameters are chosen as $R_{n,m} = R_{1,1} = 10\ \mu m$, $k_{n,m} = k_{1,1} = 0.5$, $L_{1,n} = L_{2,n} = \pi R_{1,1}$, $n_{\rm eff} = 1.5$, and $\alpha_{\rm l} = \alpha_{\rm r} = 0$. Various

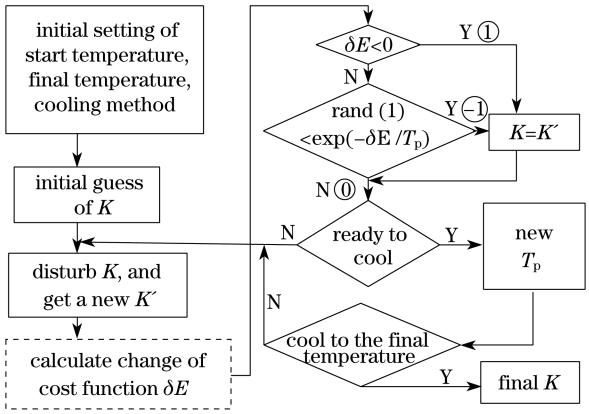

Fig. 2. Flow chart of the simulated annealing algorithm for tailoring the spectrum. Labels 1, 0, and −1 represent different acceptance and rejection states of the disturbed value during the cooling process.

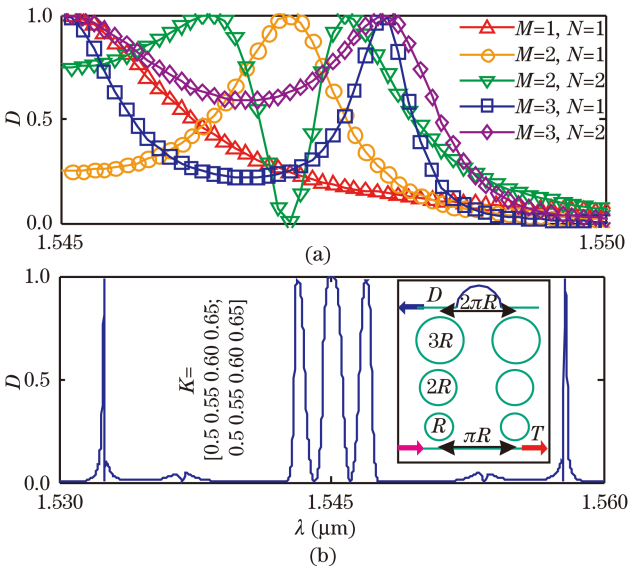

Fig. 3. Spectra of (a) MRAs with different rows and columns and (b) a MRA with different coupling coefficients, ring sizes, and waveguide lengths. Inset shows the schematic diagram of a 3×2 MRA.

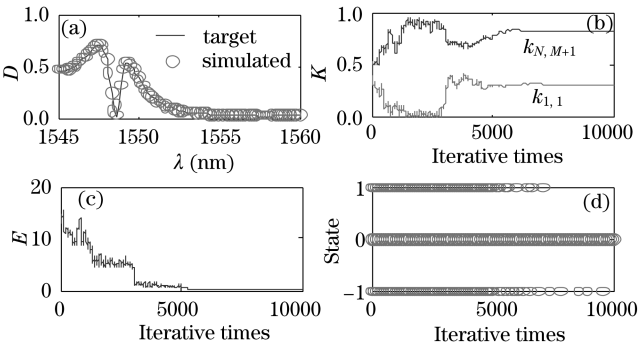

Fig. 4. Validation of the simulated annealing algorithm using a 2×2 MRA. (a) Target and simulated spectra. (b) Coupling coefficients k_{11} and $k_{N,M+1}$, (c) cost function, and (d) acceptance and rejection states during the cooling process.

transmission spectra of these configurations are caused by different constructive and destructive interference pathways. And these spectra can find different applications based on their shapes. The sharp transmission shape can be used as high-sensitivity sensors such as the MRA of $M = N = 2$, while the flat transmission with a high ratio roll-off can be used as bandpass filters such as the MRA of $M = 3$ and $N = 2$. Figure 3(b) shows the transmission spectrum of a 3×2 MRA with different coupling coefficients, ring sizes, and straight waveguides. Parameters are adopted as coupling coefficients $K = [0.50\ 0.55\ 0.60\ 0.65; 0.50\ 0.55\ 0.60\ 0.65]$, ring size $R_{1:2,1:3} = [10\ 20\ 30; 10\ 20\ 30]$ (μm), waveguide lengths $L_{1:2,1} = \pi\,[10; 20]$ (μm), and other parameters the same as those in Fig. 3(a). As shown in Fig. 3(b), three wavelength transmission spectra can be obtained near 1.545 μm. Thus this configuration can be used for multi-wavelength-based applications. By optimizing the coupling coefficients and increasing the numbers of rows and columns, both ripples in the passband and lobes in the out-of-band of the spectra can be suppressed[12,14].

We then turn to tailor the spectra using the simulated annealing algorithm. The initial and final temperatures are set to be 1 and 0.5^9 respectively, with the exponential decreasing factor as 0.5. At each temperature, we choose the iterative times per temperature as 1000, which can be modified under different cases by monitoring the cooling process. The initial guess is that all the coupling coefficients are set to be 0.5. Generally, the cooling process is performed by 20 times and the best result is chosen from those local optimized results. Firstly, we present a validation of this algorithm. A 2×2 MRA is chosen with a randomly generated coupling coefficient matrix $K_{\text{target}} = [0.32\ 0.78\ 0.57; 0.45\ 0.76\ 0.82]$. Other parameters are the same as those of Fig. 3(a). After the simulated annealing algorithm is finished, the simulated result is $K = [0.32\ 0.78\ 0.57; 0.45\ 0.76\ 0.82]$, which is the same as K_{target}. Simulation results are shown in Fig. 4. The solid line in Fig. 4(a) is the target spectrum while the circle-marker line is the simulated spectrum after the cooling process. There is a good agreement between these two curves. Figure 4(b) shows two coupling coefficients k_{11} and $k_{N,M+1}$ during the cooling process. The coupling coefficients approach to be stable after the temperature decreases 5 times. Figure 4(c) shows the cost function during the cooling process, which is initially as high as 14.44 and finally as low as 2.73×10^{-14}. This suggests a high match degree of the target and simulated spectra. The acceptance and rejection states are shown in Fig. 4(d). At the beginning, all the three states for the cooling process have high possibilities, because either the cost function is high or the possibility of acceptance is high, which corresponds to a high unmatched degree of coupling coefficients. After the cooling is nearly finished, the state 0 has more possibility until the state does not change.

Then a specified shape filter is designed using the simulated annealing algorithm. The 2×3 MRA is chosen to design three kinds of filters with the spectra as [1 0 0 0], [0 1 0 0], and [0 0 1 0] like in the wavelength range from 1545 to 1550 nm. The initial guess is that all the coupling coefficients are set as 0.5. The corresponding spectrum is shown in Fig. 5(a), which shows two zero transmissions in the passband. This can be contributed to the feedforward effects combined with the mode splittings. Figures

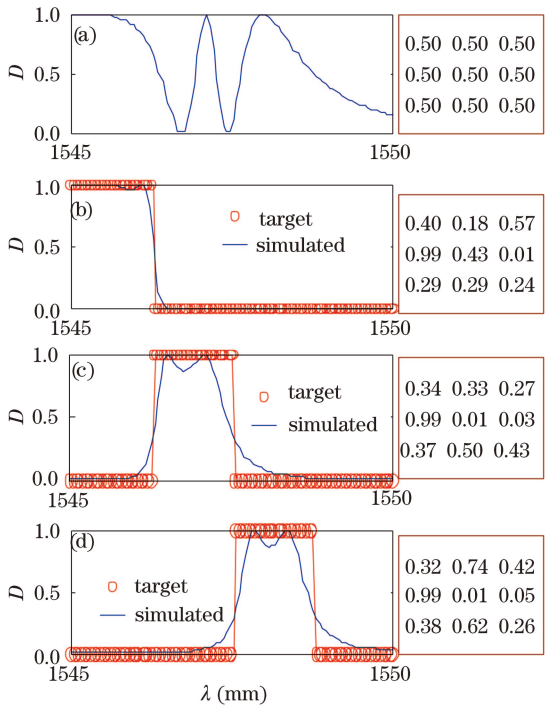

Fig. 5. (a) Spectrum under initially identical coupling coefficients as 0.5, and simulated results for (b) [1 0 0 0], (c) [0 1 0 0], and (d) [0 0 1 0] like target spectra for the configuration of 2×3 MRA.

5(b)−(d) are simulation results for [1 0 0 0], [0 1 0 0], and [0 0 1 0] like spectra. And the optimized coupling coefficients are shown in the boxes on the right. The cost functions are 1.70, 8.18, and 9.14 respectively and hence the unmatched degree increases as the passband of the target spectrum shifts away from 1545 nm.

In conclusion, we have proposed an approach based on six transfer cells and simulated annealing algorithm for the analysis and optimization of MRAs with arbitrary coupling coefficients and ring sizes. After developing the model of six transfer cells and the flow chart of the simulated annealing, several configurations are demonstrated. Due to its intuitive, fast, and intelligent calculations, this approach can be used to simulate and design MRAs with various transmission spectra for different filtering and sensing applications.

This work was supported by the National Natural Science Foundation of China under Grant No. 60577007.

References

1. A. Yariv, Electron. Lett. **36,** 321 (2000).
2. X. Zhang, X. Zhang, W. Hong, and D. Huang, Electron. Lett. **42,** 1095 (2006).
3. X. Han, F. Liu, F. Pang, F. Chu, H. Cai, R. Qu, and Z. Fang, Chin. Opt. Lett. **4,** 393 (2006).
4. Q.-Z. Huang, J.-Z. Yu, S.-W. Chen, X.-J. Xu, W.-H. Han, and Z.-C. Fan, Chin. Phys. B **17,** 2562 (2008).
5. X.-W. Dong, S.-H. Lu, S.-C. Feng, O. Xu, and S.-S. Jian, Chin. Phys. B **17,** 1029 (2008).
6. M. A. Popović, T. Barwicz, M. R. Watts, P. T. Rakich, L. Socci, E. P. Ippen, F. X. Kärtner, and H. I. Smith, Opt. Lett. **31,** 2571 (2006).
7. V. R. Almeida, C. A. Barrios, R. R. Panepucci, and M. Lipson, Nature **431,** 1081 (2004).
8. Q. Xu, B. Schmidt, S. Pradhan, and M. Lipson, Nature **435,** 325 (2005).
9. C.-Y. Chao and L. J. Guo, Appl. Phys. Lett. **83,** 1527 (2003).
10. F. Xia, M. Rooks, L. Sekaric, and Y. Vlasov, Opt. Express **15,** 11934 (2007).
11. R. Grover, V. Van, T. A. Ibrahim, P. P. Absil, L. C. Calhoun, F. G. Johnson, J. V. Hryniewicz, and P.-T. Ho, J. Lightwave Technol. **20,** 872 (2002).
12. Y. M. Landobasa, S. Darmawan, and M.-K. Chin, IEEE J. Quantum Electron. **41,** 1410 (2005).
13. B. Xia and L. R. Chen, Opt. Express **14,** 6619 (2006).
14. X. Zhang, D. Huang, W. Hong, and X. Zhang, Acta Opt. Sin. (in Chinese) **27,** 1585 (2007).
15. S. Kirkpatrick, C. D. Gelatt, Jr., and M. P. Vecchi, Science **220,** 671 (1983).